RESEARCH ARTICLE

Influence of molecular vibration on enhancements in high-order above-threshold ionization of hydrogen molecules

Stefan Pieper[a][*] and Manfred Lein[b]

[a]*Max-Planck-Institut für Kernphysik, Saupfercheckweg 1, 69117 Heidelberg, Germany*
[b]*Institut für Physik, Universität Kassel, Heinrich-Plett-Straße 40, 34132 Kassel, Germany*

Single ionization of hydrogen and deuterium molecules in strong laser pulses is studied by numerical integration of the time-dependent Schrödinger equation. We investigate the effect of the molecular vibrational energy scale on the yield in the rescattering plateau of above-threshold ionization spectra. Strong correlations between ejected electrons and the vibrational motion of the remaining ions are found.

Keywords: molecules, strong-field ionization, above-threshold ionization, channel closing

1. Introduction

Atoms or molecules exposed to intense laser fields tend to absorb more photons than needed to overcome the ionization barrier. This effect is known as above-threshold ionization (ATI) (*1, 2*). Electrons that are directly excited into the continuum can have a maximum kinetic energy of $2\,U_\mathrm{p}$, whereas a single rescattering event with the core can lead to energies up to $10\,U_\mathrm{p}$ (*3–5*). Here, the quantity U_p is the average kinetic energy of a free electron with zero drift velocity oscillating in the laser field and is called the ponderomotive potential. It is the minimum average energy a free electron can have in the presence of a laser field. In the rescattering plateau between $2\,U_\mathrm{p}$ and $10\,U_\mathrm{p}$, experimental observations (*6, 7*) and calculations (*8–14*) show that changing the laser intensity by only a few percent can lead to order-of-magnitude enhancements in yield for certain groups of peaks. Attempts to explain these effects were made in terms of multiphoton resonances with Rydberg states (*8, 9, 15*) or via the quantum path model (*10, 11, 16*). A very detailed analysis can be found in (*17*), where two different kinds of enhancements have been identified and explained as interferences of long quantum orbits. At least one of these two types can be directly related to channel closings which take place when the energy of the lowest ATI peak coincides with a certain effective threshold (*10, 11*). Since the ATI peaks are ponderomotively shifted towards lower energies with increasing laser intensity, the channel closing can be controlled by adjusting the laser intensity.

So far all published work on this effect has been related to *atoms* in laser fields. We found that the vibrational motion of *molecules* can have a striking effect on ATI channel closings. In this work, hydrogen and deuterium molecules are investigated and compared with atoms. Since these simple linear molecules provide a nuclear degree of freedom, an additional energy scale is involved in the dynamics. We show that due to the coupling between electron motion and nuclear motion, *intrinsic* channel-closing effects can be observed. ATI electron spectra decomposed into contributions belonging to different

---

[*]Corresponding author. Email: stefan.pieper@mpi-hd.mpg.de

vibrational states of the remaining ion reveal channel-closing effects upon variation of the vibrational quantum number while the laser intensity remains fixed. This is to be contrasted with atoms where the laser intensity (or laser frequency) needs to be varied in order to observe channel closings.

2.   Theoretical Background

The minimum average kinetic energy of an (otherwise free) electron in a laser field with amplitude F_0 and frequency ω is equal to the ponderomotive potential (atomic units are used unless stated otherwise) $U_{\rm p} = F_0^2/4\omega^2$, which is the energy resulting from the free oscillation of the electron. Therefore, the laser field modifies the ionization threshold. In non-resonant n-photon ionization of an atom, the ejected electron carries the final kinetic energy

$$E_{\rm kin} = n\,\omega - I_{\rm p} - U_{\rm p}, \tag{1}$$

with the atomic ionization potential $I_{\rm p}$ and integer n. It is now possible to determine the minimum number s of photons needed for full ionization as $s = {\rm ceil}[(I_{\rm p} + U_{\rm p})/\omega]$. Raising $U_{\rm p}$ via the laser intensity and therefore shifting the ionization threshold to higher photon numbers leads to the disappearance of the first ATI peak in the spectrum. As this happens, a certain s'-photon-channel is closed, which leads to an increased probability of finding the electron near the core (*8*). This situation is favourable for rescattering and certain groups of peaks within the rescattering plateau of the ATI spectrum are enhanced. Unfortunately, due to the long-range Coulomb potential, the precise intensity at which this effect takes place cannot be predicted via application of Eq. (1) alone (*10, 11, 17*).

In the case of molecules, electrons and nuclei are coupled by their Coulomb interaction so that vibrationally excited states of the ion are occupied after a strong-field ionization process. This amounts to the assumption that Eq. (1) is changed to

$$E_{\rm kin} = n\,\omega - I_{\rm p} - U_{\rm p} - \Delta E^v \tag{2}$$

for a given vibrational state with quantum number v. Here, $\Delta E^v = E^v - E^0$ is the difference in vibrational energy between the vibrationally excited state in question and the vibrational ground state of the ion. In this molecular case, it should be noted that $I_{\rm p}$ is the adiabatic ionization potential, i.e., the difference between the ground-state energies of molecule and ion, including the motion of the nuclei.

3.   Numerical model

We model the H_2 (or D_2) molecule as composed of a single active electron interacting with the core which is allowed to vibrate. Both degrees of freedom (electron coordinate and inter-nuclear distance) are treated only in one dimension, since for strong, short laser pulses, the electron is essentially driven along the laser field and the timescale for rotational motion of the whole molecule is much longer than the ultrashort pulse durations considered here. The alignment of the molecular axis was chosen orthogonal to the laser polarisation direction. This removes the dipole coupling between between the ground and first excited state of the ion (*18*) and allows the ion to be vibrationally excited to very high

v without dissociation through bond softening. This leads to the Hamiltonian

$$\widehat{H}(t) = -\frac{1}{2}\left(\frac{1}{\mu_{\mathrm{n}}}\frac{\mathrm{d}^2}{\mathrm{d}R^2} + \frac{1}{\mu_{\mathrm{e}}}\frac{\mathrm{d}^2}{\mathrm{d}z^2}\right) \\ + V_{\mathrm{n}}(R) + V_{\mathrm{int}}(z,R) + E(t)z, \tag{3}$$

where the operator $E(t)z$ with $E(t) = F(t)F_0\sin(\omega t)$ describes the interaction of the active electron with the electric field of a linearly polarised laser pulse in length gauge. F_0 is the maximum field amplitude and $F(t)$ defines the pulse shape. The electron coordinate and inter-nuclear distance are denoted by z and R; μ_{e} and μ_{n} denote the reduced masses of the active electron and of the two nuclei, respectively. The repelling nuclei are screened by the second (inactive) electron, which we assume to remain always in the energetically lowest possible state. The inter-nuclear potential is thus taken to be the exact Born-Oppenheimer ground-state potential of the molecular ion,

$$V_{\mathrm{n}}(R) = V_{\mathrm{BO}}^{\mathrm{H_2}^+}(R). \tag{4}$$

The electron-ion interaction is modelled via the soft-core potential

$$V_{\mathrm{int}}(z,R) = -\frac{1}{\sqrt{z^2 + \sigma^2(R)}}. \tag{5}$$

This choice expresses that since the electron moves perpendicular to the nuclei, there is only one single Coulomb well, whose strength is dependent on the inter-nuclear separation and the screening. The parameter $\sigma(R)$ is adjusted such that the Born-Oppenheimer ground state potential of the model Hamiltonian matches the exact Born-Oppenheimer ground-state potential of H_2 given in (*19*). A similar fitting procedure has been used previously to reproduce the Born-Oppenheimer potential of H_2^+ in a 1D model (*20*). Obviously, this model allows only for single ionization of the molecule. There is no dissociation channel included, and the second electron is completely passive in its ground state, so that only one reaction channel (namely single ionization) is modelled.

For comparison, we also carry out calculations for a 1D atom. The atomic Hamiltonian reads

$$\widehat{H}_{\mathrm{atom}}(t) = -\frac{1}{2\mu_e}\frac{\mathrm{d}^2}{\mathrm{d}z^2} + V_{\mathrm{int}}(z) + E(t)z, \tag{6}$$

where the Coulomb interaction between electron and nucleus was modelled as a simple soft-core potential,

$$V_{\mathrm{int}}(z) = \frac{1}{\sqrt{z^2 + a}}. \tag{7}$$

The soft-core parameter was adjusted to $a = 1.4863$, such that the ionization potential I_{p} of the atom equals the one for H_2

The 2D wave function is propagated via the split-operator method combined with 2D Fourier transformations. The two-dimensional grid (z-spacing 0.36 a.u., R-spacing 0.05 a.u.) extends in R-direction from 0.2 a.u. to 12.95 a.u., in electronic direction from -276.3 a.u. to 276.3 a.u., corresponding to 256 and 1536 grid points, respectively. In the electronic dimension, the grid is further extended up to $|z| = 2522.7$ a.u. to allow for the possibility of large electronic excursions and to obtain high-resolution energy spectra for the ATI electrons. This is done via splitting the wave function (*21*): in the overlap

region between inner and outer grid, we decompose the 2D wave function $\Psi_{\text{out}}(z, R, t)$ repeatedly into a single sum of product states, i.e.,

$$\Psi_{\text{out}}(z, R, t) = \sum_j \xi_j(z, t)\zeta_j(R, t), \tag{8}$$

where $\xi_j(z, t)$ and $\zeta_j(R, t)$ are so-called canonical basis states or natural orbitals (*22*). They can be calculated as eigenvectors of the one-particle density matrices for each of the two coordinates z and R. We chose the number of expansion terms such that all terms add up to a probability of at least 0.999. No more than four terms were needed in each expansion. In the outer part of the 2D grid, the coupling between the two degrees of freedom is neglected: the interaction potential $V_{\text{int}}(z, R)$ is replaced by the R-independent potential $V_{\text{out}}(z) = V_{\text{int}}(z, R = 2)$. This allows us to apply 1D propagations separately to the functions $\xi_j(z, t)$ and $\zeta_j(R, t)$, and grid extensions up to several thousands atomic units become feasible. In contrast to (*21*), the potential is gradually changed between $|z| = 10 \dots 161$ a.u. from V_{int} to V_{out} to avoid discontinuities of the Hamiltonian. Each time the wave function is on the verge of hitting one of the inner grid boundaries, one has to introduce a new "layer" in the outside part (i.e. an additional set of product states) containing the decomposed wave function from the overlap region. Hence the size of the overlap region, the transfer timing and the number of layers are subtle parameters which have to be carefully chosen. On the winning side we have huge electronic grids that are capable of keeping the whole probability on the grid, even after strongly ionizing pulses.

For the atomic calculation, a 1D grid with no grid splitting was applied. We used the same electronic grid spacing and applied the same propagation scheme.

The pulse shape $F(t)$ is chosen such that the temporal pulse integral vanishes. The five-cycle pulses (molecules) and nine-cycle pulses (atom) used in this work are ramped on and off following a $\sin^2$ envelope over 1.5 cycles and have a mid plateau with constant intensity that extends over two cycles for the molecular case and six cycles for the atomic case. Three cycles without laser field are added (ten cycles in the atomic calculation) to let the ejected electrons move further away from the Coulomb potential of the core. We have checked that finally no significant Coulomb energy is carried by the ATI electrons considered in this work. The laser wavelength is 800 nm so that we have $I_{\text{p}} = 10.0\,\omega$ for all three systems considered. (For the atomic calculation, the soft-core parameter was adjusted such that I_{p} is the same as in the H_2 case.) The system is regarded as ionized for $|z| > 30$ a.u. The precise choice of this value is not important since the results shown in this work involve electrons driven at least 500 a.u. from the ion at the end of the simulation.

4. Results

The kinetic-energy spectra of ATI electrons are analyzed into contributions corresponding to different vibrational states v of the remaining ion. This is done via projection of the ionized part Ψ_{ion} (i.e., where $|z| > 30$ a.u., see above) of the wave function at the end of the simulation onto the different vibrational states χ_v of the ion,

$$\phi_v(z) = \int \chi_v^*(R)\,\Psi_{\text{ion}}(z, R, t_{\text{end}})\,\mathrm{d}R. \tag{9}$$

The modulus squared, $|\widetilde{\phi}_v(p_z)|^2$, of the Fourier transform is then rescaled from momentum to energy. In this way we obtain one ATI spectrum for each vibrational state. In this work, Ψ_{ion} contains only the right-going part of the final wave function.

According to Eq. (2), the ATI peaks in these spectra are shifted by ΔE^v. Scanning through different v and thus varying ΔE^v can therefore lead to channel closings. Since ΔE^v can easily exceed the photon energy within the first few vibrational states (for the H_2^+ ion and $\lambda = 800$ nm, $\Delta E^7 \approx 1.0\,\omega$ and for the D_2^+ ion, $\Delta E^9 \approx 0.96\,\omega$), a channel closing will almost certainly be observed within the first nine vibrational states, no matter where exactly the first ATI peak is located. So instead of scanning through different laser intensities, in the case of molecules one can also "scan" through different vibrational states of the remaining ion. With growing quantum number v the vibrational energy gets larger, so at some v, the lowest-possible channel is closed, and we expect the corresponding energy spectrum to show the characteristic channel-closing features known from atoms. The difference to atoms is that the energy is scanned in discrete steps of hard-wired, non-equidistant size. We compare ionization of H_2 and D_2. In the case of D_2^+ ions, the closer-lying vibrational states allow for a less coarse scanning in energy already for low vibrational states, and we expect a clearer resolution of the observed features as compared to H_2^+.

Strong-field single ionization by a laser field of suitable intensity leads to a channel closing according to Eq. (1). In Fig. 1, ATI electron spectra are shown for ionization of the three model systems under investigation: atom, molecular hydrogen and molecular deuterium (top to bottom). In the latter two cases, projections onto the $v = 4$ vibrational state of the molecular ion are taken. In each case, two different intensities are plotted, with $0.4\,\omega$ difference in U_p. The two corresponding curves are vertically shifted with respect to each other to enhance visibility. For each species, the upper curve (lower intensity) shows a dip in the rescattering plateau (located before the final big hump), while the lower curve shows the maximum yield in the rescattering plateau within the intensity range under investigation. Clearly, the enhancement effect known from atoms (upper panel) can be identified for the case of molecules as well. The full molecular spectra (the sum over contributions from all v, not shown here) do not as clearly show the effect, because the channel-closing intensity depends on the vibrational state. In the projections on individual vibrational states, Fig. 1, the effect is clearly visible. However, depending on the distribution of vibrational states, in general there will be one major contribution to the total spectrum by one specific v, which is then responsible for a noticeable enhancement even in the complete spectrum. Applying Eqs. (1) and (2), the channel closing is expected at intensities 7.89×10^{13} W/cm^2 ($n = 13$) or 1.05×10^{14} W/cm^2 ($n = 14$) for the atom, 8.82×10^{13} W/cm^2 for H_2 and 9.19×10^{13} W/cm^2 for D_2 (ionic state $v = 4$ and $n = 14$ in both cases) As known from earlier publications, this does not exactly match the observation, i.e., the concept of energy conservation alone cannot explain the effect quantitatively. Due to the different vibrational energies in hydrogen and deuterium, according to Eq. (2) it is expected that in case of D_2 more laser intensity is needed for the channel closing to take place. For $v = 4$, the difference in ΔE^4 amounts to $0.17\,\omega$, which would have to be compensated by a correspondingly higher U_p. In fact, the maximum enhancement for D_2 is found at a higher intensity with a value of U_p higher by $0.1\,\omega$. (Note that U_p was sampled in steps of $0.1\,\omega$.)

In Fig. 2, envelopes of ATI spectra are plotted for molecular hydrogen and molecular deuterium. Seven and nine different projections on vibrational states of the ion are shown, respectively, so that in both cases approximately the same range of vibrational energy is covered, namely about one laser photon energy. The laser intensity is fixed at 9.435×10^{13} W/cm^2, and the variation in vibrational energy ΔE^v plays the role of the changing laser intensity in the case of Fig. 1. According to Eq. (2), again a channel closing takes place. Clearly, the resulting effect is visible in both H_2 and D_2. The spectra have been divided by the total yield of the respective vibrational states to avoid confusion of the channel closing effect with changes due to higher or lower total occupation of vibrational states. The effect is still visible if unnormalized spectra are considered, but is strongly
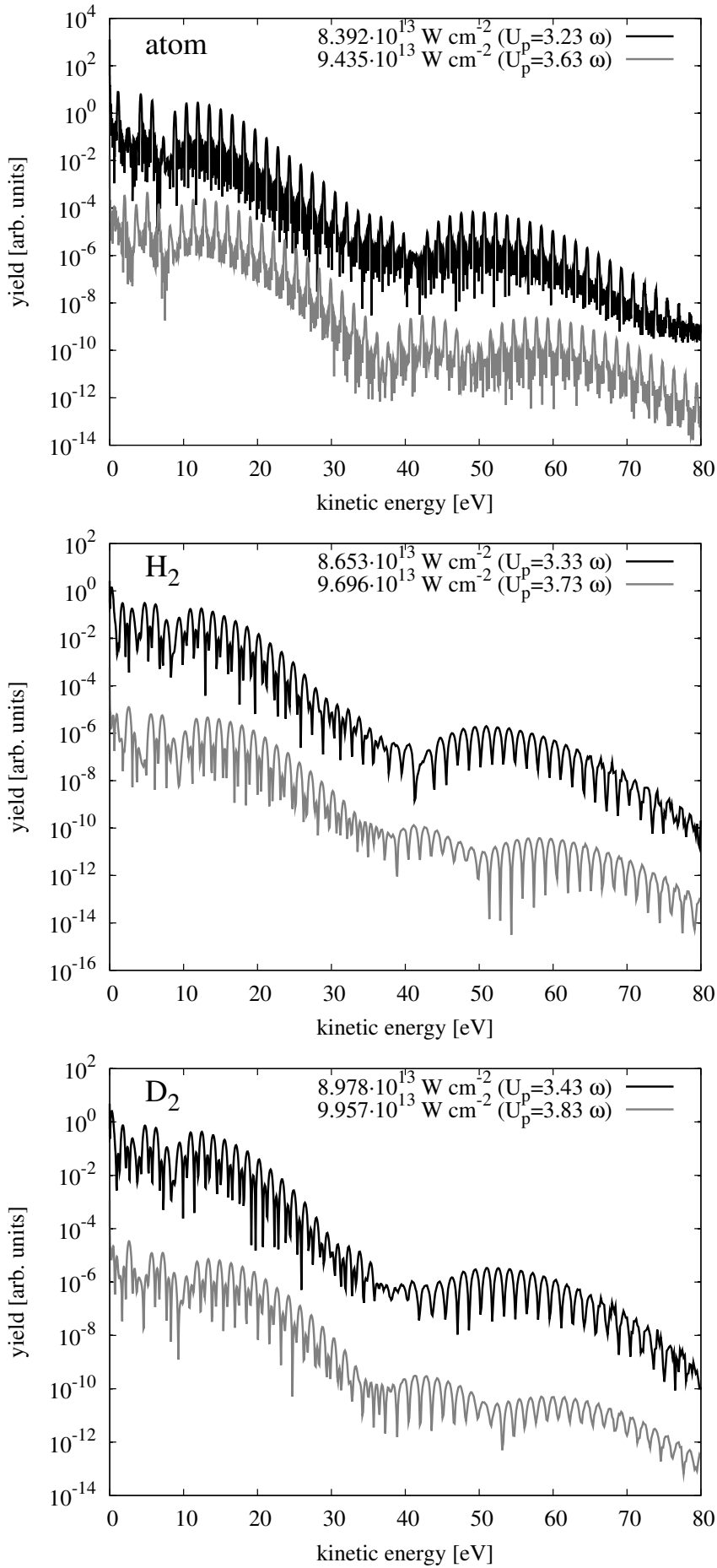
S. Pieper and M. Lein

Figure 1. Kinetic-energy spectra of (right-going) ATI electrons in the case of the 1D atom (upper panel), H_2 (central panel), and D_2 (lower panel). For the molecular cases, the $v = 4$ projection is shown. Two different laser intensities are plotted in each case to visualise the intensity-dependent enhancement of the rescattering plateau. In each panel, one of the two spectra has been vertically shifted by a factor of 5×10^4 to improve readability.
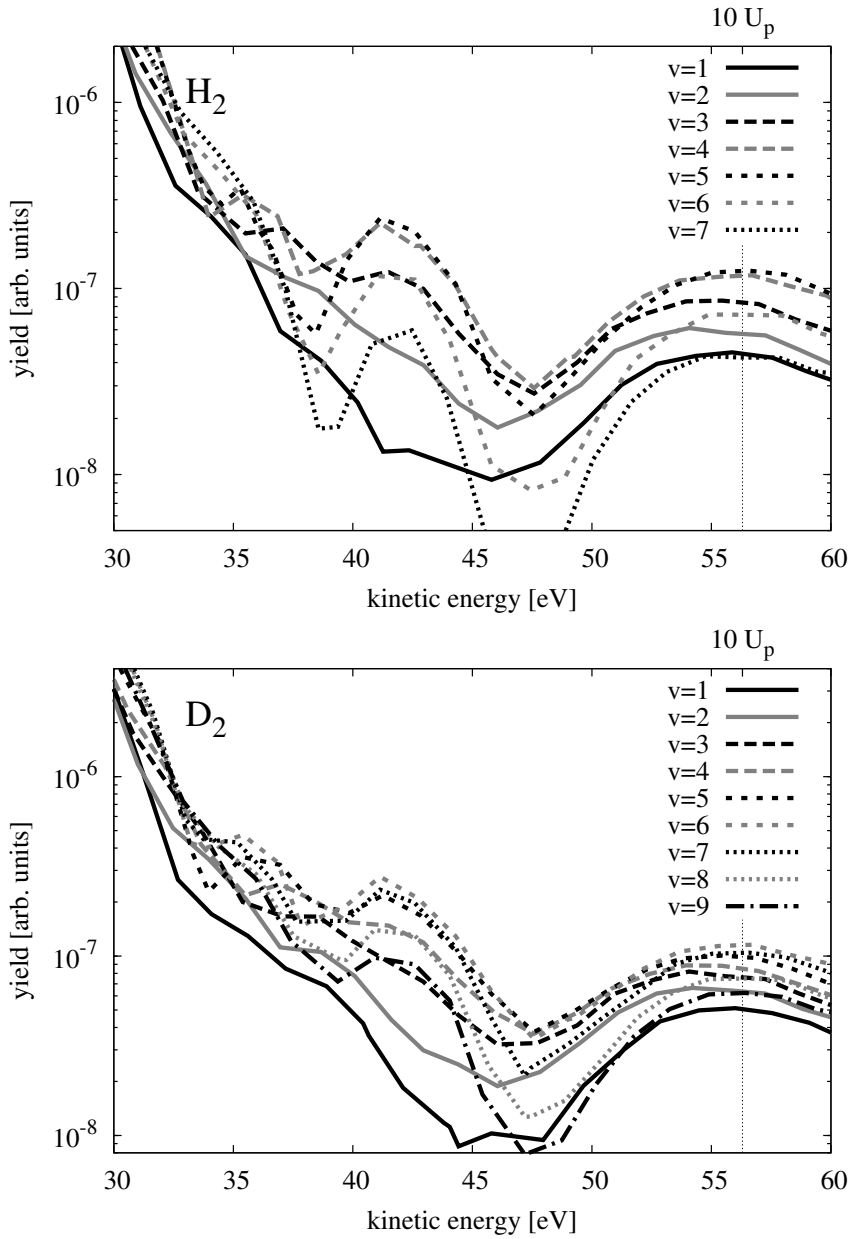
Figure 2.   Envelopes of kinetic-energy spectra of (right-going) ATI electrons in the case of H_2 (upper panel), and D_2 (lower panel). The laser intensity is 9.435×10^{13} W/cm^2 ($U_p = 3.63\ \omega$). Projections on several different vibrational states of the remaining ion are plotted to show the intrinsic channel-closing effect. Each spectrum has been divided by the total yield of the respective vibrational state to clearly isolate the channel-closing effect from the v-dependence of the total yield.

masked by a general trend prescribed by the vibrational state distribution. For example, in the top-left panel of Fig. 3, which shows the total distribution of vibrational states for the same laser intensity as in Fig. 2, the population decreases quickly as a function of v around $v = 4$. For the case of H_2, it is obvious from Fig. 2 (upper panel) that the highest yield is found for the $v = 4$ and $v = 5$ projections, i.e, the channel closing occurs somewhere between these two vibrational energies. For D_2, the highest yield is clearly reached for $v = 6$ already, maybe a little later, as the $v = 7$ curve is still quite close by. This fits perfectly the relative comparison in energy conservation, since $\Delta E_{H_2^+}^4 = 0.64\ \omega$ and $\Delta E_{H_2^+}^5 = 0.78\ \omega$, whilst $\Delta E_{D_2^+}^6 = 0.68\ \omega$ and $\Delta E_{D_2^+}^7 = 0.78\ \omega$. A coarse estimation, supported by both examples, would suggest that the vibrational energy needed for an exact closing is about $0.7\ \omega$. In any case, H_2 and D_2 exhibit a clear difference in the behaviour of
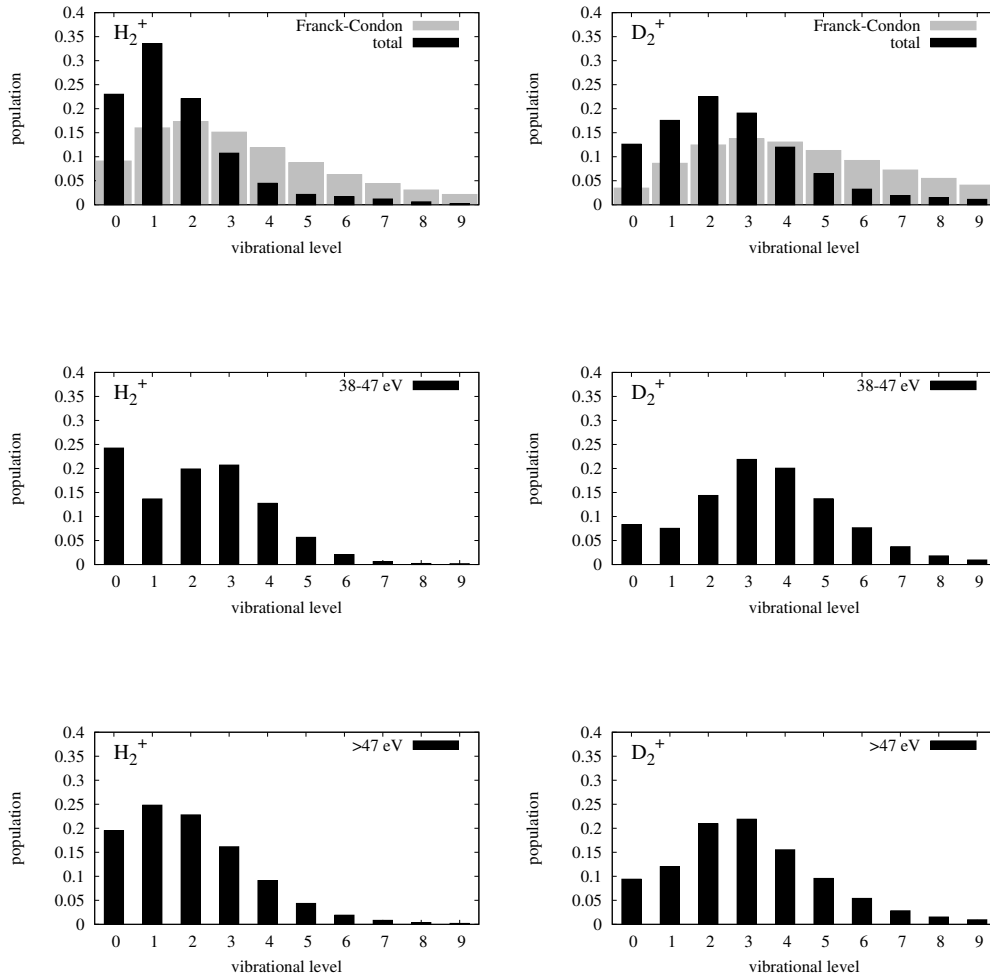
Figure 3.   Occupation of vibrational states of H_2^+ (left column) and D_2^+ (right column) after single ionization of the respective molecule with laser intensity 9.435×10^{13} W/cm^2 ($U_p = 3.63\,\omega$). Three cases are shown: including all ATI electrons (upper two panels), including only electrons with kinetic energies between 38 and 47 eV (two central panels), and including only electrons with more than 47 eV (lower two panels). The uppermost panels show in grey the Franck-Condon distribution for comparison.

the plateau enhancement, namely with changing v, it happens much more slowly in the D_2 case as compared to H_2, supporting the connection to the concept of energy conservation. Yet the application of Eq. (2) predicts the channel closing at $\Delta E^v \approx 0.37\,\omega$, which does obviously not quantitatively match the observation.

In Fig. 3, the population of vibrational states $v = 0$ to $v = 9$ is plotted for the cases of H_2 (left column) and D_2 (right column) after ionization with a laser intensity of 9.435×10^{13} W/cm^2. From top to bottom, different energy windows have been applied to the corresponding ATI electrons. The two upper panels show the total vibrational distribution of the produced ions for all right-going electrons. In the background, for comparison the Franck-Condon distribution is shown in grey for both cases. In the lower four panels, yields within restricted electron energy windows are shown. Here, the bars show unnormalized distributions, i.e., the underlying ATI spectra have not been normalized.

If one restricts the spectra to ATI electrons with kinetic energy in a certain interval, e.g. between 38 eV and 47 eV in the middle panel of Fig. 3, the distribution of vibrational states is very different from the total distribution. It is significantly warmer, i.e., the maximum and average are shifted towards higher v, especially for the case of D_2^+. Since the
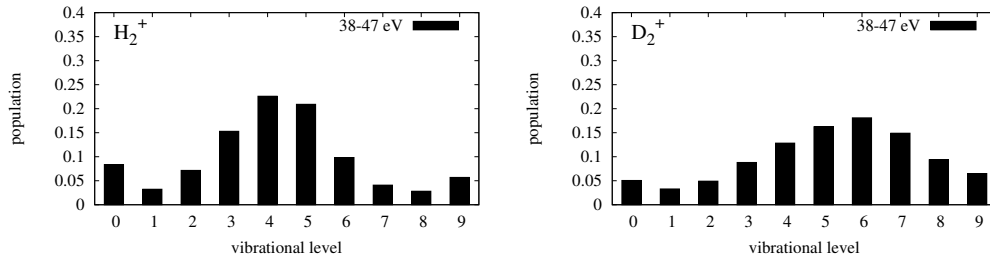
Figure 4.   Occupation of vibrational states of $H_2{}^+$ (left panel) and $D_2{}^+$ (right panel) after single ionization of the respective molecule with laser intensity 9.435×10^{13} W/cm^2 ($U_p = 3.63\,\omega$) including ATI electrons with kinetic energies between 38 and 47 eV. The bars show normalized distributions, i.e, the full spectrum was divided by the total yield of the respective vibrational states (i.e. these distributions belong to the envelopes shown in Fig. 2).

chosen energy window matches the rescattering plateau of the ATI spectrum, the distributions show that for rescattered electrons higher vibrational excitation of the corresponding ion is favoured. In the lower two panels, ATI electrons with energies above 47 eV are chosen. The corresponding distribution of vibrational states changes again. The distributions resemble more the total distributions shown in the uppermost panel.

For comparison, the bars of Fig. 4 correspond to the spectra of Fig. 2 and therefore belong to normalized spectra, i.e., the yield for each vibrational state has been divided by the total yield of the vibrational state. This was done to avoid masking of the channel-closing effect by the total distribution over the vibrational states. In other words, if the yield falling within the chosen electron energy window followed the same dependence on v as the total yield (upper panel of Fig. 3), then this normalized distribution would be constant. Instead, one clearly sees a preference of highly excited vibrational states, exactly matching the observation of maximum enhancement within Fig. 2 as expected.

For the present laser intensity, the windowed electrons (which lie in the rescattering plateau) give comparatively hot vibrational distributions, while the lower vibrational states are mainly found as partners of *direct* electrons. Generally speaking, a strong correlation between the kinetic energy of the ATI electrons and the vibrational state of the corresponding ion is obvious.

5.   Conclusions

Our calculations show that spectral enhancements observed at certain laser intensities in strong-field ionization of atoms can also be found in strong-field ionization of molecules. The vibrational motion of the nuclei in the cases of H_2 and D_2 can play the role of applying different laser intensities in the atomic case. Energy conservation serves as a simple explanation of the observed channel-closing effect, yet cannot completely determine at which laser intensity (or vibrational quantum number) it will take place. The difference between H_2 and D_2 is well explained by the different spacing of the vibrational levels. Furthermore, strong correlations between the nuclear motion and the kinetic energy of the ATI electrons is found. These correlations are revealed by the vibrational distributions of the ions for specific energy intervals of the ATI electrons. On the experimental side, to observe the predicted effect, coincidence measurements will be necessary. The distribution of vibrational states in the $H_2{}^+$ ion after strong-field ionization of H_2 has been successfully measured already (*18*), but it still seems difficult to make such a measurement selectively for electrons of given kinetic energies.

References

(1) Agostini, P.; Fabre, F.; Mainfray, G.; Petite, G.; et al. Free-Free Transitions Following Six-Photon Ionization of Xenon Atoms. *Phys. Rev. Lett.* **1979**, *42*, 1127.

(2) Eberly, J.H.; Javanainen, J.; Rzążewski, K. Above-threshold ionization. *Phys. Rep.* **1991**, *204*, 331.

(3) Paulus, G.G.; Nicklich, W.; Xu, H.; Lambropoulos, P.; et al. Plateau in above threshold ionization spectra. *Phys. Rev. Lett.* **1994**, *72*, 2851.

(4) Paulus, G.G.; Becker, W.; Nicklich, W.; et al. Rescattering effects in above-threshold ionization: a classical model. *J. Phys. B* **1994**, *27*, L703.

(5) Paulus, G.G.; Becker, W.; Walther, H. Classical rescattering effects in two-color above-threshold ionization. *Phys. Rev. A* **1995**, *52*, 4043.

(6) Hansch, P.; Walker, M.A.; Van Woerkom, L.D. Resonant hot-electron production in above-threshold ionization. *Phys. Rev. A* **1997**, *55*, R2535–R2538.

(7) Hertlein, M.P.; Bucksbaum, P.H.; Muller, H.G. Evidence for resonant effects in high-order ATI spectra. *J. Phys. B* **1997**, *30*, L197.

(8) Muller, H.G.; Kooiman, F.C. Bunching and Focusing of Tunneling Wave Packets in Enhancement of High-Order Above-Threshold Ionization. *Phys. Rev. Lett.* **1998**, *81*, 1207.

(9) Muller, H.G. Numerical simulation of high-order above-threshold-ionization enhancement in argon. *Phys. Rev. A* **1999**, *60*, 1341.

(10) Paulus, G.G.; Grasbon, F.; Walther, H.; Kopold, R.; et al. Channel-closing-induced resonances in the above-threshold ionization plateau. *Phys. Rev. A* **2001**, *64*, 021401(R).

(11) Kopold, R.; Becker, W.; Kleber, M.; et al. Channel-closing effects in high-order above-threshold ionization and high-order harmonic generation. *J. Phys. B* **2002**, *35*, 217.

(12) Popruzhenko, S.V.; Korneev, P.A.; Goreslavski, S.P.; et al. Laser-Induced Recollision Phenomena: Interference Resonances at Channel Closings. *Phys. Rev. Lett.* **2002**, *89*, 23001.

(13) Wassaf, J.; Véniard, V.; Taïeb, R.; et al. Strong Field Atomic Ionization: Origin of High-Energy Structures in Photoelectron Spectra. *Phys. Rev. Lett.* **2003**, *90*, 013003.

(14) Krajewska, K.; Fabrikant, I.I.; Starace, A.F. Threshold effects in strong-field detachment of H^- and F^-: Plateau enhancements and angular distribution variations. *Phys. Rev. A* **2006**, *74*, 053407.

(15) Potvliege, R.M.; Vučić, S. High-order above-threshold ionization of argon: Plateau resonances and the Floquet quasienergy spectrum. *Phys. Rev. A* **2006**, *74*, 023412.

(16) Kopold, R.; Becker, W.; Kleber, M. Quantum path analysis of high-order above-threshold ionization. *Opt. Commun.* **2000**, *179*, 39.

(17) Milošević, D.B.; Hasović, E.; Busuladžić, M.; Gazibegović-Busuladžić, A.; et al. Intensity-dependent enhancements in high-order above-threshold ionization. *Phys. Rev. A* **2007**, *76*, 053410.

(18) Urbain, X.; Fabre, B.; Staicu-Casagrande, E.M.; de Ruette, N.; Andrianarijaona, V.M.; Jureta, J.; Posthumus, J.H.; Saenz, A.; Baldit, E.; et al. Intense-Laser-Field Ionization of Molecular Hydrogen in the Tunneling Regime and Its Effect on the Vibrational Excitation of H_2^+. *Phys. Rev. Lett.* **2004**, *92*, 163004.

(19) Kołos, W.; Szalewicz, K.; Monkhorst, H.J. New Born-Oppenheimer potential energy curve and vibrational energies for the electronic ground state of the hydrogen molecule. *J. Chem. Phys.* **1985**, *84*, 3278.

(20) Feuerstein, B.; Thumm, U. Fragmentation of H_2^+ in strong 800-nm laser pulses: Initial-vibrational-state dependence. *Phys. Rev. A* **2003**, *67*, 043405.

(21) Grobe, R.; Haan, S.L.; Eberly, J.H. A split-domain algorithm for time-dependent multi-electron wave functions. *Comp. Phys. Comm.* **1999**, *117*, 200.

(22) Löwdin, P.O. Quantum Theory of Many-Particle Systems. I. Physical Interpretations by Means of Density Matrices, Natural Spin-Orbitals, and Convergence Problems in the Method of Configurational Interaction. *Phys. Rev.* **1955**, *97*, 1474.